Check for updates

Received: 11 May 2022 | Revised: 22 July 2022 | Accepted: 6 September 2022

DOI: 10.1002/eqe.3744

WILEY

RESEARCH ARTICLE

Hybrid simulation of a partial-strength steel–concrete composite moment-resisting frame endowed with hysteretic replaceable beam splices

Roberto Andreotti | **Giulia Giuliani** | **Nicola Tondini** | **Oreste S. Bursi**

Department of Civil, Environmental and Mechanical Engineering, University of Trento, Trento, Italy

Correspondence
Nicola Tondini, Department of Civil, Environmental and Mechanical Engineering, University of Trento, Trento, Italy.
Email: nicola.tondini@unitn.it

Funding information
European Union; Italian Ministry of Education, University and Research; MIUR; Departments of Excellence, Grant/Award Number: L232/2016; Research Fund of Coal and Steel DISSIPABLE, Grant/Award Number: 800699

Abstract

This paper deals with the seismic response assessment of a steel–concrete moment-resisting frame (MRF) equipped with special dissipative replaceable components (DRCs): the dissipative replaceable beam splices (DRBeS), which combine large energy dissipation with ease of replacement. The evaluation of the full potential of DRBeS requires a system-level investigation, that is, a six-story MRF, whereby the hysteretic effects of beam splices partial-strength joints are considered on the global response of the structural system. Therefore, an OpenSees finite element (FE) frame model, based on previous experimental campaigns with cyclic displacements on partial-strength joints, and a Matlab model validated on OpenSees, were used for a more complex experimental activity via hybrid simulation (HS). The aim of the simulations was twofold: (i) to increase knowledge of the non-linear behaviour of steel-concrete composite partial-strength MRFs; and (ii) to study the effectiveness of the DRBeS components for increasing the recovery of functionality after a major seismic event. Therefore, to appreciate the performance of the partial-strength MRF at damage limitation (DL), significant damage (SD) and near collapse (NC) within the performance-based earthquake engineering (PBEE) approach, HSs were carried out. In such instances, the ground floor was physically tested at full scale in the laboratory and the remainder of the structure was numerically simulated. Relevant results showed that the DRBeS were capable of dissipating a significant amount of hysteretic energy and of protecting the non-dissipative parts of partial-strength joints and the overall structure with an ease of replacement.

KEYWORDS
ease of replacement, full-scale tests, hybrid simulation, hysteretic component, low-damage components, steel–concrete composite structure, seismic performance

This is an open access article under the terms of the Creative Commons Attribution-NonCommercial-NoDerivs License, which permits use and distribution in any medium, provided the original work is properly cited, the use is non-commercial and no modifications or adaptations are made.
© 2022 The Authors. *Earthquake Engineering & Structural Dynamics* published by John Wiley & Sons Ltd.

10969845, 0, Downloaded from https://onlinelibrary.wiley.com/doi/10.1002/eqe.3744 by CochraneItalia, Wiley Online Library on [03/11/2022]. See the Terms and Conditions (https://onlinelibrary.wiley.com/terms-and-conditions) on Wiley Online Library for rules of use; OA articles are governed by the applicable Creative Commons License

1 INTRODUCTION

1.1 Background and motivation

Steel and steel–concrete composite structures performance under seismic loading has long been regarded as very effective due to material ductility, construction lightweight and structural systems versatility.[1,2] Moreover, the aforementioned structures are expected to offer increasingly safe solutions, as innovations such as replaceable parts, self-centering systems, easy supplemental damping, isolation devices and economic loss control have been unveiled and put into practice.[3] However, joint design plays a major role in structural detailing and systematically affects the system behaviour so that members and joint design must occur simultaneously and iteratively. Such complexity is usually regarded as an obstacle for designers; especially under the encompassing legal constraints imposed by design standards. For instance, partial-strength joints cannot be used in seismic steel or steel–concrete composite structures in Italy.[4] Conversely, they can be used in the European standards.[5–7] As regards USA standards, composite partially restrained moment frames (C-PRMF) are allowed, where beam-to-column joints can experience yielding in ductile zones, with a minimum rotation capacity of 20 mrad.[8] Nevertheless, several analysis/design requirements are present in the AISC standard, with the inclusion of a pre-qualification requirement based on experimental tests. A similar approach is present in Japanese standards; the Building Standard Law and the Architectural Institute of Japan issued laws, notifications and recommendations, for the plastic design of structures and joints that render partial-strength joints not popular in Japan, see, for instance the Standard Specifications for Steel and Composite Structures.[9] More precisely and differently from European standards, the massive use of welding render joints to be full strength with dissipative zones at beam ends. Thus, due to both promising developments and solutions including the presence of PBEE,[10] the design and adoption of innovative steel and steel–concrete composite partial-strength joints constitute a research gap also for regulation frameworks.

With regard to experimental activities conducted in Europe, USA and Japan, tests focused on steel and steel–concrete composite partial-strength joints subjected to cyclic tests were performed and see, among others.[1,11–13] Moreover, several joints tested in Japan were properties of construction companies, with the primary goal to validate specific joint details. Thus, limited tests and mainly pre-qualified data are available and are little amenable to generalization.

Also the application of the PBEE approach[10] entails two major consequences on structural design. The first one regards that both structures and joints must cope with different limit states and relevant seismic inputs. Therefore, and in line with the seismic European Standard,[5,6] hereinafter, damage limitation (DL), significant damage (SD) and near collapse (NC) limit states need to be satisfied. The second one, instead, as the capability of localizing and limiting seismic-induced damage in the spirit of passive control.[14] Most of the investigations involving passive control are concerned with elastic behaviour of the load-bearing structure and dissipation in damping devices. Nonetheless, in recent years, low-damage design has attracted much attention; for instance, the use of friction connections that dissipate large amounts of energy without experiencing high damage was proposed by several authors.[15–17] Other devices were conceived to reduce damage in steel structures, such as slit dampers, that were experimentally tested both for eccentrically braced frames (EBFs)[18] and MRF[19]: it was demonstrated that they can provide wide and compact hysteretic behaviour both in force–displacement and moment–rotation diagrams. Regarding MRF structural schemes, among others, Koetaka et al.[20] tested hysteretic dampers for connections along the weak axis of the columns, which also exhibited stable and effective hysteretic behaviour.

Along that main vein, also the ease of replacement was an issue. Thus, the results of several European research projects devoted to the conception of new type of connections, capable of dissipating large amounts of energy and being easily replaceable were collected in the dissemination project INNOSEIS.[21] In particular, an extensive experimental campaign analysed the behaviour of dissipative braced pinned connections in the INERD project.[22] Another dissipative device analysed in depth within the FUSEIS project,[23] namely FUSEIS type 2, consisted of an innovative dissipative replaceable connection for composite MRF. Nonetheless, also these novel solutions were commonly tested at the joint assembly level and their performance on large-scale specimens was rarely investigated because of budget and/or facility constraints.

As anticipated, beam-to-column assemblies were generally tested under idealized loads and boundary conditions. As they do not reflect actual situations, it is natural to resort to hybrid simulations (HSs) where also partial-strength joints can be investigated at the system level with realistic loading histories.[24–26] For clarity, HS is a powerful tool that enables to reproduce the seismic response of full-scale structures by sub-dividing the structural system to be tested into a physical and a numerical part. The physical sub-structure (PS), which contains the elements, whose seismic behaviour is being investigated, is physically tested in the laboratory, while the numerical sub-structure (NS) is simulated in a computational environment that runs in parallel to the experimental test. Coupling between the PS and NS is guaranteed by imposing

10969845, 0, Downloaded from https://onlinelibrary.wiley.com/doi/10.1002/eqe.3744 by CochraneItalia, Wiley Online Library on [03/11/2022]. See the Terms and Conditions (https://onlinelibrary.wiley.com/terms-and-conditions) on Wiley Online Library for rules of use; OA articles are governed by the applicable Creative Commons License

continuity at a few selected interface DOFs, common to both sub-domains. To this aim, electro-hydraulic actuators are employed to impose displacements to the PS. Many experimental projects demonstrated the effectiveness of this structural testing method also in complex systems like bridges, where hysteresis must be taken into account both in the PS and the NS.[27,28]

1.2 | Research scope and core contribution

On these premises and to crystallize the ideas, there is the need: (i) to seek for energy dissipation in MRFs of a building with minimum downtime and functionality loss; (ii) to comprehensively evaluate the effectiveness of novel solutions within passive control based on the outcomes of full-scale HSs. These are the aims of the Research Fund for Coal and Steel (RFCS) DISSIPABLE project[29]; it is a European-funded pilot project which intended to experimentally demonstrate through large-scale shaking table and HSs the effectiveness of improved dissipative components easily replaceable also when subjected to strong seismic records.

To work with a consistent nomenclature, the joints examined in the DISSIPABLE project are conceived as dissipative replaceable components (DRCs), and each component, namely INERD, FUSEIS type 1 and FUSEIS type 2, are named as dissipative replaceable braced connection (DRBrC), dissipative replaceable link frame (DRLF) and dissipative replaceable beam splices (DRBeS). At the Materials and Structures Testing laboratory (LPMS) of the University of Trento, Italy, five full-scale steel frames, representative of five 6-storey-building prototypes endowed with the aforementioned components were tested by means of the HS method. In such a context, the innovative contribution provided by the tests conducted at UNITN is twofold: (i) to explore the interaction of joint components with the irreplaceable parts of the frame; indeed, the proposed experimental/numerical activity provided large full-scale testing data at the frame level and not at the component level; (ii) to account for the large geometry of the frame and to simulate realistic seismic loadings by means of a PBEE approach; thus, a modern HS method was employed. The research work comprehensively describes the outcomes of the HSs performed on a full-scale frame equipped with DRBeS components.

2 | CHARACTERISTICS OF THE DRBeS COMPONENT

The DRBeS component shown in Figure 1, was conceived for steel–concrete composite MRFs and designed in such a way to concentrate plastic deformations in steel plates. This was achieved by cutting the composite beam in a region close to a beam-to-column joint; then, both bending and shear continuity were re-established by means of steel plates connected to the lower flange and web of the steel profile. To avoid cracking of the concrete slab during a seismic event, two layers of reinforcement bars are introduced and are continuous through the concrete slab gap. The amount of reinforcement area is oversized and, thus, the neutral axis is forced to lie between the two reinforcement bar layers; as a result, the highest deformations are concentrated in the replaceable plates, rather than the reinforcement bars. Experimental campaigns and numerical studies were conducted at IST Lisbon (Calado et al.[30,31]) and at Politecnico of Milan (Castiglioni et al.,[32] Kanyilmaz et al.[33,34]). They demonstrated the effectiveness of such a joint in the dissipation of hysteretic energy through large moment–rotation cycles and in the prevention of structural damage in other structural components. As a result, the possible repair work is limited to the replacement of the fuse plates.

With respect to the mechanical behaviour of the device, both numerical studies and analytical formulations showed that the strength capacity is governed by the buckling behaviour of the plates under hogging moments. This failure mode entails loss of strength and stiffness, prevents the plates to exploit their full hardening capacity and introduces asymmetry in the joint response. The plate resistance to the beam resistance ratio defines the capacity ratio α, which is a parameter of primary importance for the design of innovative frames equipped with DRBeS components. An important outcome of the aforementioned experimental campaigns consisted: (i) in setting a lower bound of α, in order to exhibit high bending resistance and energy dissipation; in identifying an upper bound for α to ensure that damage does not affect any component or member that is intended to remain elastic. Thus, the following ranges of α, that is, $0.60 < \alpha^{+} < 0.75$ and $0.30 < \alpha^{-} < 0.50$, are suggested for sagging (α^{+}) and hogging (α^{-}) bending moments,[32] respectively. A comparison between bolted and welded beam splices was performed by Valente et al.[35]; they observed that bolted fuses exhibit high bending resistance and are capable of dissipating large amount of plastic energy, whilst welded fuses show comparatively high values of elastic stiffness. Moreover, experiments clearly showed how replaceability is in general easier in the case of bolted

10969845, 0, Downloaded from https://onlinelibrary.wiley.com/doi/10.1002/eqe.3744 by CochraneItalia, Wiley Online Library on [03/11/2022]. See the Terms and Conditions (https://onlinelibrary.wiley.com/terms-and-conditions) on Wiley Online Library for rules of use; OA articles are governed by the applicable Creative Commons License

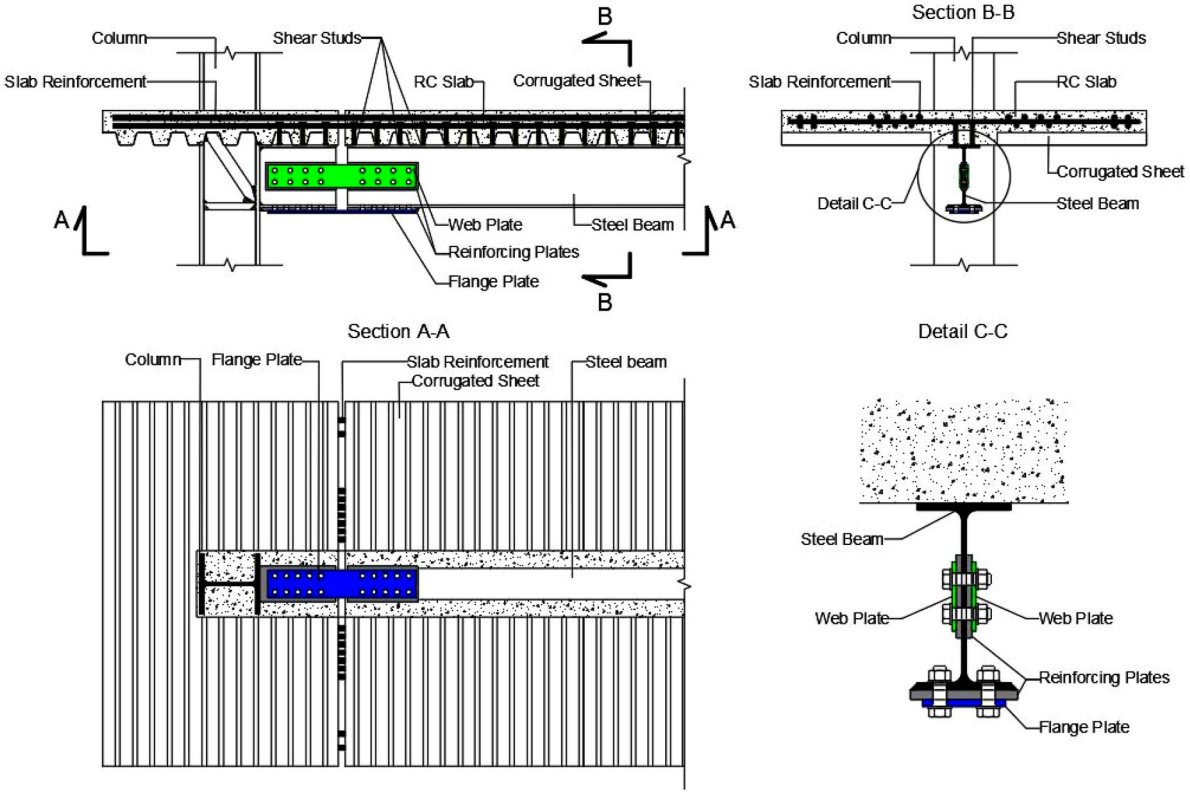


FIGURE 1 Transversal and top view of the partial-strength joint with the DRBeS components

fuses. In sum, the bolted solution was preferred due to high energy dissipation capability and replacement ease of steel plates.

3 | DESIGN OF THE PROTOTYPE BUILDING

Within the RFCS DISSIPABLE project, it was agreed to design and test a six-storey building prototype in the laboratory by means of HS. The structural scheme was endowed with a hybrid lateral-resisting system characterized by two-span MRFs equipped with DRBeS in one direction and three-span concentrically braced frames (CBF) equipped with DRBrC in the other direction. The span length was 4.275 m with an inter-storey height of 3.5 m. The structural steel was selected to be S355 for all the elements, but for the fuse plates of the DRBeS, that were made of S235 (EN 1993-1-1[36]). The seismic design of the 3D building was performed by means of linear multi-modal analysis with response spectrum at the DL and at the SD limit states according to EN 1998-1.[5] The provisions derived from the INNOSEIS project[21] were employed to design both the DRBeS and DRBrC components, whilst the remainder of the structure was designed according to the Eurocodes (EN 1993-1-1,[36] EN 1993-1-8,[37] EN 1994-1-1[38] and EN 1998-1[5]).

The main frame characteristics are reported in Table 1, while Tables 2 and 3 collect the dimensions of the building dissipative components. The bolted column-base joints and the welded beam-to-column joints were designed as rigid and full strength in accordance with EN 1993-1-8[37] and the capacity design criterion.[5] The composite section of the beams was made of an IPE 270 steel section and a concrete slab 150-mm thick with a C25/30 strength class, for which a 55-mm high corrugated steel sheeting was adopted. The composite action was obtained by means of Nelson studs, which ensure full shear connection between the steel profile and the composite slab. Both transverse reinforcements – ϕ 16 mm – of composite slab and shear studs – $\phi \frac{5}{8}''$ – were designed according to EN1994-1-1.[38] The DRBeS joints were located at the ends of the two composite beams. The steel plates that compose the fuse connection were connected to beams by means of high strength friction bolts designed according to EN1993-1-8.[37] To ensure an effective moment transmission between composite beams and columns under earthquake loading, additional transverse reinforcements were added close to beam-to-column joints to fulfil the provisions of Annex C of EN1998-1.[5]

10969845, 0, Downloaded from https://onlinelibrary.wiley.com/doi/10.1002/eqe.3744 by CochraneItalia, Wiley Online Library on [03/11/2022]. See the Terms and Conditions (https://onlinelibrary.wiley.com/terms-and-conditions) on Wiley Online Library for rules of use; OA articles are governed by the applicable Creative Commons License

TABLE 1 Column and beam cross sections of the physical sub-structure

Floor number	Element	Profile
1–2	Perimetral column	HE 260 B
3–4–5	Perimetral column	HE 240 B
6	Perimetral column	HE 220 B
1–2	Internal column	HE 300 B
3–4–5	Internal column	HE 280 B
6	Internal column	HE 260 B
1–2	Braces	HE 140 A
3–4–5	Braces	HE 120 A
6	Braces	HE 100 A
All floors	Beam MRF	IPE 270 + 150-mm composite deck
All floors	Beam CBF	IPE 300

TABLE 2 Width and thickness dimensions in millimetres of DRBeS plates for the whole building

Floor number	Flange plate	Web plate
1–2–3	120 × 10	100 × 6
4	100 × 10	100 × 6
5–6	100 × 8	100 × 6

TABLE 3 DRBrC component dimensions in millimetres for the whole building

Floor number	Pin diameter	Chamfering
1–2	45	5
3–4	40	5
5–6	35	5

To perform preliminary analyses and to investigate the performance of the partitioned algorithm to be employed for HS, a reference 3D non-linear FE model of the building was developed in OpenSees.[39,40] In particular, linear beam–column elements were employed for beams, columns and braces; conversely, non-linear two-node links with *Pinching4* material[39,41] were adopted for modelling DRBeS and DRBrC components. The parameters used to describe the monotonic backbone curve of both the DRBeS and DRBrC components were computed through the analytical formulas provided by the INNOSEIS provisions.[21] Furthermore, the whole hysteretic behaviour was calibrated by fitting the cyclic behaviour obtained from experiments on both DRBeS, provided in Calado et al.,[31] and the DRBrC, performed within the DISSIPABLE project, respectively. The calibration procedure of the OpenSees constitutive models was carried out by means of the software Multical,[42] and can be found in Andreotti et al.[40]

The HS was carried out on a plane frame that represents the ground floor and part of the first floor, whilst the remainder of the structure was numerically simulated. In such instances, a representative 2D FE model able to well approximate the structural behaviour of the 2D frame within the whole building was deemed necessary. Moreover, since only two DOFs were controlled in the HS, as illustrated in Figure 2, a sub-structured model of the 2D frame was conceived.[40] On these premises, consistency between the 3D building prototype, the 2D monolithic frame and the 2D sub-structured frame models was verified by means of modal, pushover and time-history analyses. In this respect, Table 4 collects the first four periods relevant to the DBReS component direction for the aforementioned models; while Figure 2B depicts a comparison of the pushover responses. Moreover, the P-Δ effects were also investigated and relevant comparisons showed that discrepancies were negligible. Thus, it was decided to not apply the axial loads to the columns in the PS. Thereby, the 2D sub-structured frame model was considered suitable to represent the global 3D building behaviour and was, therefore, employed in the HS. Since the control of rotational DOFs at boundaries between the NS and PS is a hard task to perform by means of hydraulic actuators, only the horizontal translational DOFs were controlled at the column mid-height, assumed

10969845, 0, Downloaded from https://onlinelibrary.wiley.com/doi/10.1002/eqe.3744 by CochraneItalia, Wiley Online Library on [03/11/2022]. See the Terms and Conditions (https://onlinelibrary.wiley.com/terms-and-conditions) on Wiley Online Library for rules of use; OA articles are governed by the applicable Creative Commons License

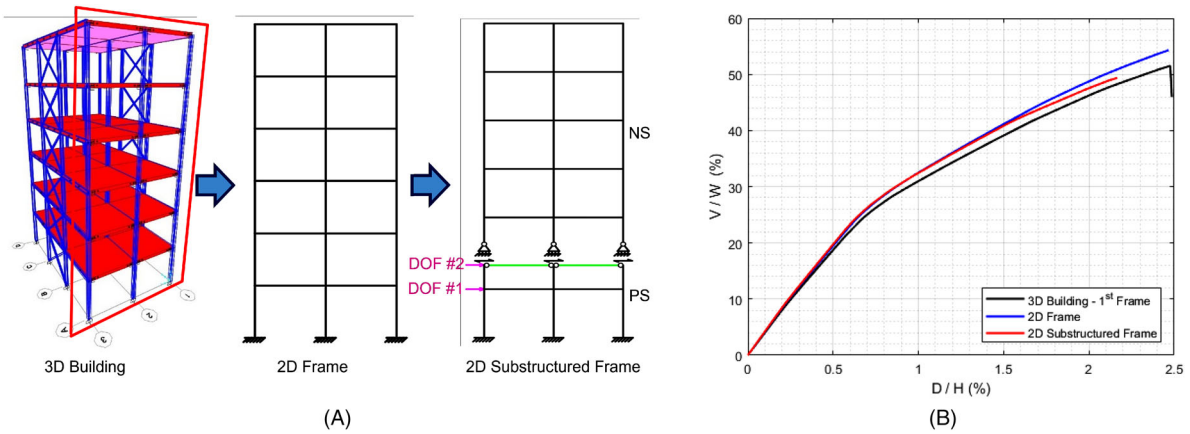


FIGURE 2 (A) Sub-structuring of the prototype building; (B) relevant validation by means of pushover analyses

TABLE 4 Comparison of dynamic periods among different structural models

Mode	3D building	2D frame	2D sub-structured frame	Hybrid simulation
	T (s)	*T* (s)	*T* (s)	*T* (s)
1	1.42	1.38	1.32	1.35
2	0.44	0.44	0.42	0.42
3	0.24	0.25	0.25	0.25



FIGURE 3 Conception of the hybrid simulation

to be inflection points. Finally, as an additional comparison/validation, the periods identified by means of preliminary HS results are also reported in Table 4.

4 | CHARACTERISTICS OF THE PHYSICAL SUB-STRUCTURE

A schematic representation of the HS is depicted in Figure 3, while Figure 4 includes the experimental test setup. One can observe that the PS extends from the base to exactly halfway of the first and the second floor, whilst the remainder of the structure is reproduced by the NS. The test setup includes the first floor of the six-storey frame, with columns extended for 1.75 m above the floor level. For the sake of clarity of the test results presented in Section 7, the load cell of the actuator MOOG #1 depicted in Figure 3B acquires the external load force acting at the first floor, whilst the force values read by MOOG #2 represent the total shear force at the second floor. The PS consisted of three steel columns 5.65 m high, two composite beams located at 3.5 m from the ground and characterized by a span length of 4.275 m. To reproduce the rigid

10969845, 0, Downloaded from https://onlinelibrary.wiley.com/doi/10.1002/eqe.3744 by CochraneItalia, Wiley Online Library on [03/11/2022]. See the Terms and Conditions (https://onlinelibrary.wiley.com/terms-and-conditions) on Wiley Online Library for rules of use; OA articles are governed by the applicable Creative Commons License

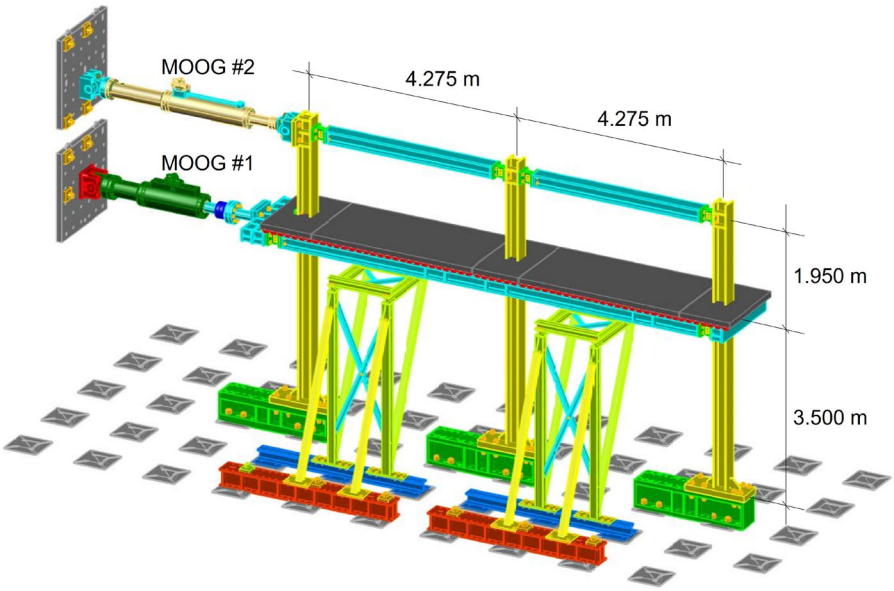


FIGURE 4 The PS with the relevant testing equipment

TABLE 5 Mechanical properties of S355 steel profiles

Property	HE 260 B	HE 220 M	IPE 270
Yield strength f_y (MPa)	382	439	394
Ultimate strength f_u (MPa)	540	604	523
Elongation at failure (%)	33	29	29

TABLE 6 Mechanical properties of S235 steel plates

Property	$t = 6$ mm	$t = 10$ mm
Yield strength f_y (MPa)	251	259
Ultimate strength f_u (MPa)	441	408
Elongation at failure (%)	33	29

diaphragm effect, two axially stiff HE 220 M steel profiles were positioned in parallel to the frame. Such beams, depicted in Figure 3, were connected to the frame by means of pinned hinges. Moreover, two lateral frames guaranteed the out-of-plane stability as shown in Figure 3. The actual mechanical properties of all the materials are reported in Tables 5–8. The instrumentation was employed to measure global and local quantities such as the horizontal displacement at each DOF as well as local strains, relative displacements and absolute rotations in specific points of the structure, mainly close to the DRBeS. Both Figures 5 and 6 schematically depict the whole configuration of the sensors installed on the specimen. The dissipative components were numbered from Conn #1 to #4. Three sections of each composite beam, outside of the

TABLE 7 Mechanical properties of B450C reinforcement bars

Property	Φ16	Φ18	Φ20	Φ22
Yield strength f_y (MPa)	521	528	532	529
Ultimate strength f_u (MPa)	615	619	623	633
Elongation (%)	11.6	13.5	10.3	12.1

TABLE 8 Cubic compressive strength of concrete C25/30

Property	Cube 1	Cube 2	Cube 3	Cube 4	Cube 5	Average
R_c (MPa)	48.3	47.1	55.0	50.3	49.0	49.4

10969845, 0, Downloaded from https://onlinelibrary.wiley.com/doi/10.1002/eqe.3744 by CochraneItalia, Wiley Online Library on [03/11/2022]. See the Terms and Conditions (https://onlinelibrary.wiley.com/terms-and-conditions) on Wiley Online Library for rules of use; OA articles are governed by the applicable Creative Commons License

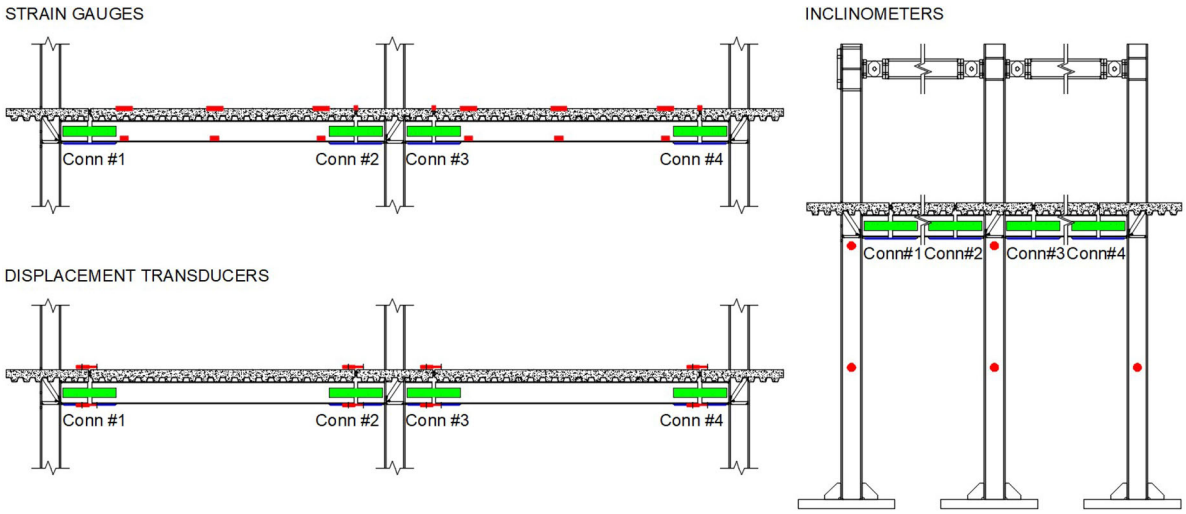


FIGURE 5 Sensor layout

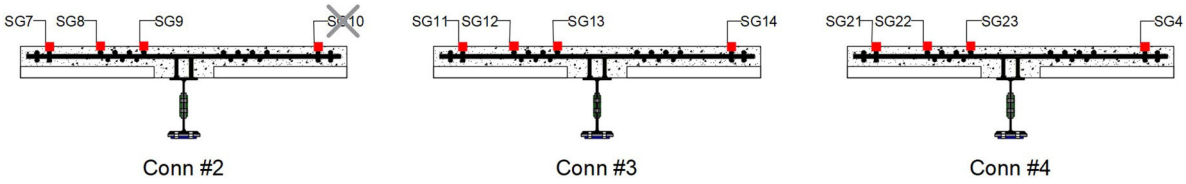


FIGURE 6 Location of strain gauges on the reinforcement bars



FIGURE 7 Some photos of the sensor equipment

expected plastic deformation zone, were instrumented with strain gauges on the lower part of the steel profile web and on the top of the concrete slab, as illustrated in Figure 7. For the former, the strain gauges were located on the web rather than the flange to avoid the influence of shear-lag effects. Based on an elastic behaviour and plane sections, the curvature was then calculated as

$$\chi = \frac{\varepsilon_{top} - \varepsilon_{bot}}{H_{sec}} \tag{1}$$

where ε_{top} and ε_{bot} are the strains measured at the top and at the bottom of the composite section and H_{sec} defines the height of the cross section. Hence, the bending moment M on each instrumented section located in the elastic range

10969845, 0, Downloaded from https://onlinelibrary.wiley.com/doi/10.1002/eqe.3744 by CochraneItalia, Wiley Online Library on [03/11/2022]. See the Terms and Conditions (https://onlinelibrary.wiley.com/terms-and-conditions) on Wiley Online Library for rules of use; OA articles are governed by the applicable Creative Commons License

reads

$$M = E_s \cdot I_{cmp} \cdot \chi \tag{2}$$

where I_{cmp} defines the inertia moment of the composite section and E_s the steel Young's modulus. As a result, by neglecting the effects of gravity loads due to self-weight, the bending moment at the DRBeS cross sections was obtained by means of a linear interpolation of the bending moment values in the beam elastic region. Moreover, see Figure 7, to measure the joint rotation, two displacement transducers were placed at the concrete slab upper edge and of the lower flange of the steel profile. Thus, the rotation ϕ of the beam stub including the DRBeS was calculated as $\phi = (\Delta_{top} - \Delta_{bot})/H_{sec}$, where Δ_{top} and Δ_{bot} define the top and the bottom displacements. The bare flange plate strain was instead estimated as $\varepsilon = \Delta_{bot}/L_0$ where L_0 defines the distance between the internal bolts on each side of the DRBeS component, equal to 180 mm.

To check whether the column base undergoes plastic deformations, inclinometers were placed at different levels of the columns, as depicted in Figure 5. Thus, the measures of the absolute rotations in two different sections of the column allowed for the estimation of the bending moment at the base of the columns. In addition, to detect any possible yielding in three different DRBeS sections, strain gauges were applied to the reinforcement bars, as depicted in Figure 6. Unfortunately, strain gauge number 10 got damaged during the erection process of the frame and could not be replaced.

5 | MAIN FEATURES OF THE PARTITIONED ALGORITHM USED FOR HS

The numerical method used to perform HS is briefly described herein. In particular, the HSs were conducted by means of a partitioned algorithm based on the finite element tearing and interconnecting (FETI) method; it was implemented through the $G - \alpha$ algorithm described in Abbiati et al.[43] For clarity, the system of equations of motion can be written as

$$\mathbf{M}\,\ddot{\mathbf{u}} + \mathbf{C}\,\dot{\mathbf{u}} + \mathbf{r}(\mathbf{u}) = \mathbf{b} + \mathbf{f}, \tag{3}$$

where in a sub-structured form,

$$\mathbf{M} = \begin{bmatrix} \mathbf{M_{NN}} & \mathbf{0} & \mathbf{0} \\ \mathbf{0} & \mathbf{M_{BB}} & \mathbf{0} \\ \mathbf{0} & \mathbf{0} & \mathbf{M_{PP}} \end{bmatrix}, \mathbf{C} = \begin{bmatrix} \mathbf{C_{NN}} & \mathbf{C_{NB}} & \mathbf{0} \\ \mathbf{C_{BN}} & \mathbf{C_{BB}} & \mathbf{C_{BP}} \\ \mathbf{0} & \mathbf{C_{PB}} & \mathbf{C_{PP}} \end{bmatrix} \tag{4}$$

define, the mass and damping matrices, respectively, and

$$\mathbf{u} = \begin{bmatrix} \mathbf{u_N} \\ \mathbf{u_B} \\ \mathbf{u_P} \end{bmatrix} \quad \mathbf{r}(\mathbf{u}) = \begin{bmatrix} \mathbf{r_N}(\mathbf{u_N}, \mathbf{u_B}) \\ \mathbf{r_B}(\mathbf{u_N}, \mathbf{u_B}, \mathbf{u_P}) \\ \mathbf{r_P}(\mathbf{u_B}, \mathbf{u_P}) \end{bmatrix} \quad \mathbf{b} = \begin{bmatrix} \mathbf{0} \\ \mathbf{b_B} \\ \mathbf{0} \end{bmatrix} \quad \mathbf{f} = \begin{bmatrix} \mathbf{f_N} \\ \mathbf{f_B} \\ \mathbf{f_P} \end{bmatrix} = -\mathbf{M}\,\mathbf{i}\ddot{u}_g \tag{5}$$

are, respectively, displacements, restoring forces, interface forces and external forces vectors, while $\mathbf{i}$ is the influence vector.

Though the partitioned algorithm was implemented in a state-space form,[43] the non-linearity exhibited by the DRBeS joints was instead modelled by means of the piece-wise linear *Pinching4* material included in OpenSees software[39] and a typical output is depicted in Figure 8. As a result, due to the material model complexity and the large set of parameters involved, it was deemed necessary to implement a *Pinching4* routine in the Matlab-based algorithmic framework. As a result, to cope with the linearly implicit approach described by Abbiati et al.,[43] also the *Pinching4* follows the one predictor-one corrector logic.

From the experimental viewpoint, the laboratory is equipped with a system that is able to control at most two actuators MOOG #1 and MOOG #2 for HS in real time. Therefore, both the NS and the PS were dynamically condensed to a

10969845, 0, Downloaded from https://onlinelibrary.wiley.com/doi/10.1002/eqe.3744 by CochraneItalia, Wiley Online Library on [03/11/2022]. See the Terms and Conditions (https://onlinelibrary.wiley.com/terms-and-conditions) on Wiley Online Library for rules of use; OA articles are governed by the applicable Creative Commons License

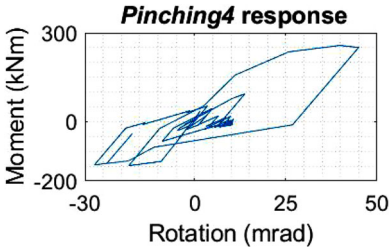


FIGURE 8 Hysteretic response of the implemented *Pinching4* routine

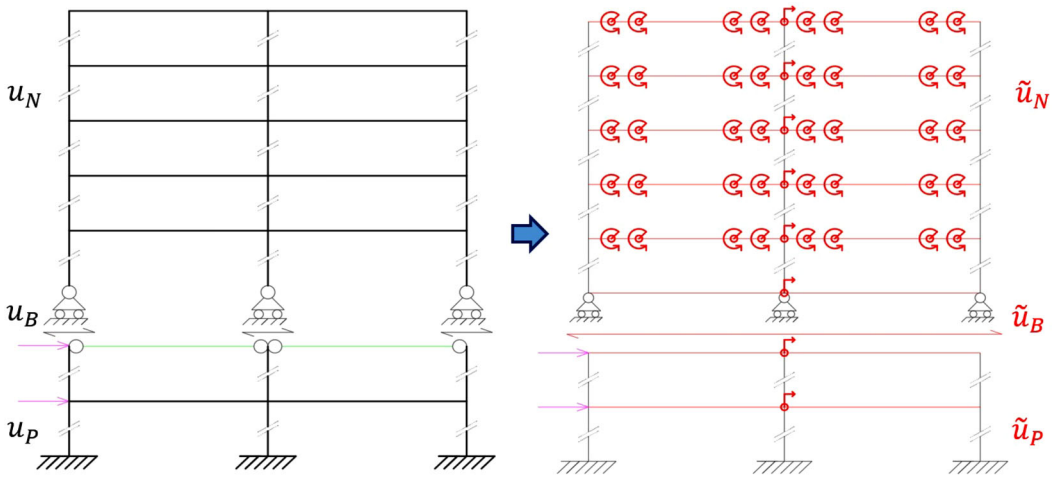


FIGURE 9 Dynamic condensation of DoFs. The reduced DoFs are highlighted in red.

reduced number of DOFs. In particular, the component mode synthesis method suggested by Craig and co-workers was utilized.[44,45] For brevity as depicted in Figure 9, hereinafter the reduction of the DOFs of the NS to six horizontal DOFs at each of the six floors and to forty rotational DOFs is described. The relevant equations read

$$\begin{bmatrix} \tilde{\mathbf{u}}_\mathbf{N} \\ \tilde{\mathbf{u}}_\mathbf{B} \end{bmatrix} = \mathbf{T}^{-1} \begin{bmatrix} \mathbf{u}_\mathbf{N} \\ \mathbf{u}_\mathbf{B} \end{bmatrix} \tag{6}$$

where $\tilde{\mathbf{u}}_\mathbf{N}$ and $\tilde{\mathbf{u}}_\mathbf{B}$ are the component generalized coordinates for numerical and boundary DOFs; u_N and u_B the component physical displacement coordinate for numerical and boundary DOFs and T the component mode matrix.

The same approach was applied for the PS. The viscous damping equal to 2% was included in the NS by means of Rayleigh's damping; whilst it was set to zero for the PS because inherently present in the PS. To govern the stability of the whole coupled system conditioned by the control of the electro-hydraulic actuators, a time-scale coefficient $\lambda = \Delta t_C / \Delta t$ was introduced to control the test time scale. As a result, the ratio between the time integration step Δt_C used to solve the system of equations of motion and the wall clock time Δt of the controller ranged between 50 and 100.

6 | GROUND MOTION SELECTION AND HS PROGRAMME

6.1 | Selection of natural records

Three tests characterized by a different return period of the seismic input were performed on the frame. Each return period corresponded to a limit state, namely DL, SD and NC, in agreement with the new proposal of EN 1998-1-8.[6] For each of the aforementioned limit states, a suite of seven triplets of accelerograms was provided; and the accelerograms were selected by means of two different criteria: (i) spectral compatibility and (ii) minimization of the discrepancy between the responses of the monolithic and the sub-structured frames depicted in Figure 2A. With regard to spectral compatibility,

10969845, 0, Downloaded from https://onlinelibrary.wiley.com/doi/10.1002/eqe.3744 by CochraneItalia, Wiley Online Library on [03/11/2022]. See the Terms and Conditions (https://onlinelibrary.wiley.com/terms-and-conditions) on Wiley Online Library for rules of use; OA articles are governed by the applicable Creative Commons License

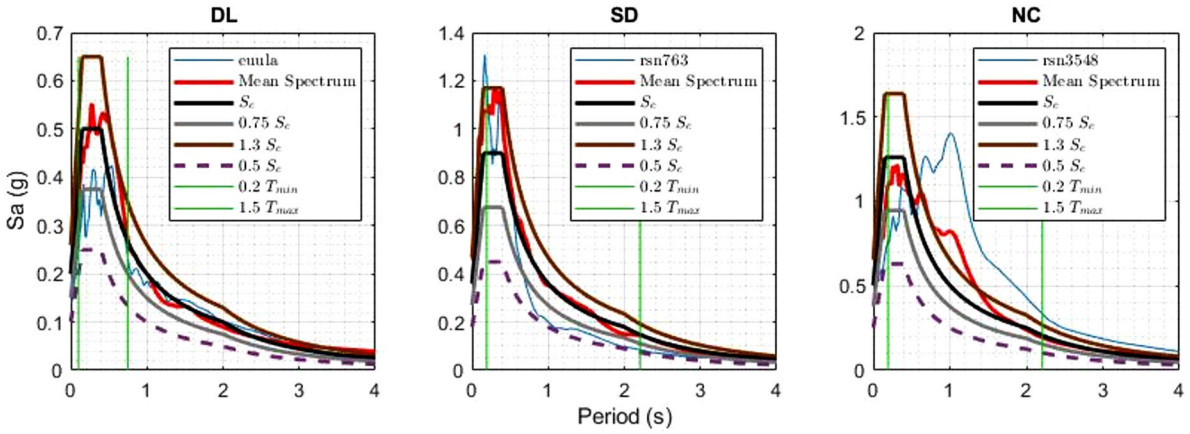


FIGURE 10 Response spectra of the selected accelerograms for the limit states DL, SD and NC. Spectral compatibility limits provided by EN 1998-1 NEN SC8 PT1[6]

since the testing frame is part of a three dimensional building, multiple ground motions were considered, as prescribed in Annex C of EN 1998-1C8.[6] Therefore, for each accelerogram, the geometric mean (GM) of the two horizontal response spectrum components was computed to verify the spectral compatibility as

$$GM = \sqrt{S_{e,X} \cdot S_{e,Y}} \tag{7}$$

where $S_{e,X}$ and $S_{e,Y}$ are the spectra of the X and Y horizontal components of the ground motion, respectively. For each limit state, Figure 10 shows the GM spectrum of the selected accelerogram, the average of the GM spectra for each suite and the limits of compatibility imposed by EN 1998-1C8, that can be summarized as follows: the compatibility is checked in the period ranges $[0.2T_{1x} - 1.5T_{1x}]$ and $[0.2T_{1y} - 1.5T_{1y}]$, where T_{1x} and T_{1y} are the fundamental periods of the structure along the two main directions. In such period ranges: (i) the average of the 5% damped response spectra, taken as the GMs of the X and Y components, shall fall between 0.75 and 1.3 times the target spectrum, considered as the elastic spectrum defined by EN 1998-1C8; (ii) the average value of the ratio between the average of GMs and the target spectrum shall be greater than 0.95; (iii) the 5% damped GM response spectrum of each accelerogram shall not fall below 50% of the target spectrum.

The requirement on spectral compatibility is fulfilled as the average value of the aforementioned ratio assumes the values of 1.00, 1.02 and 1.19, respectively, for DL, SD and NC. For both DL and SD limit states, the selected accelerogram cope with the limits imposed by EN 1998-1C8 within a significant range of periods. In this respect, Figure 10 highlights that the selected ground motion for the NC limit state is a pulse-like record and does not satisfy such limits. However, the EN 1998-1C8 allows for the use of such accelerograms, that were employed in the experimental campaign to obtain a structural damage greater than the one provided in SD tests.

To quantify the discrepancy between the monolithic frame and the sub-structured frame time-history response, the following parameters were considered:

$$Energy\ Error\,(\%) = \left|\frac{E_i - E_j}{E_j}\right| \cdot 100 \tag{8a}$$

$$NRMSE(\%) = \frac{||x_i - x_j||_2/\sqrt{N}}{x_{j,max} - x_{j,min}} \cdot 100 \tag{8b}$$

$$NENERR(\%) = \left|\frac{||x_i||_2 - ||x_j||_2}{||x_j||_2}\right| \cdot 100 \tag{8c}$$

The energy error in Equation (8a) represents a percentage difference between two scalar quantities, that is, the hysteretic energy dissipated by the devices. Conversely, both NRMSE and NENERR expressed in terms of percentage, compare two datasets, i and j, in which the j dataset is taken as a reference. More precisely, NRMSE results to be sensitive to frequency,

10969845, 0, Downloaded from https://onlinelibrary.wiley.com/doi/10.1002/eqe.3744 by CochraneItalia, Wiley Online Library on [03/11/2022]. See the Terms and Conditions (https://onlinelibrary.wiley.com/terms-and-conditions) on Wiley Online Library for rules of use; OA articles are governed by the applicable Creative Commons License

TABLE 9 Error indices between monolithic and sub-structured frame responses

Parameters (%)	DL	SD	NC
Energy error	0.46	0.43	7.06
NRMSE – base shear V_{base}	20.48	10.85	3.01
NENERR – base shear V_{base}	16.70	6.07	3.52
NRMSE – bending moment 1st *floor connection*	22.69	12.16	4.98
NENERR – bending moment 1st *floor connection*	18.10	2.54	4.49
NRMSE – displacement 1st *floor*	21.73	11.16	4.84
NENERR – displacement 1st *floor*	25.36	1.57	28.56

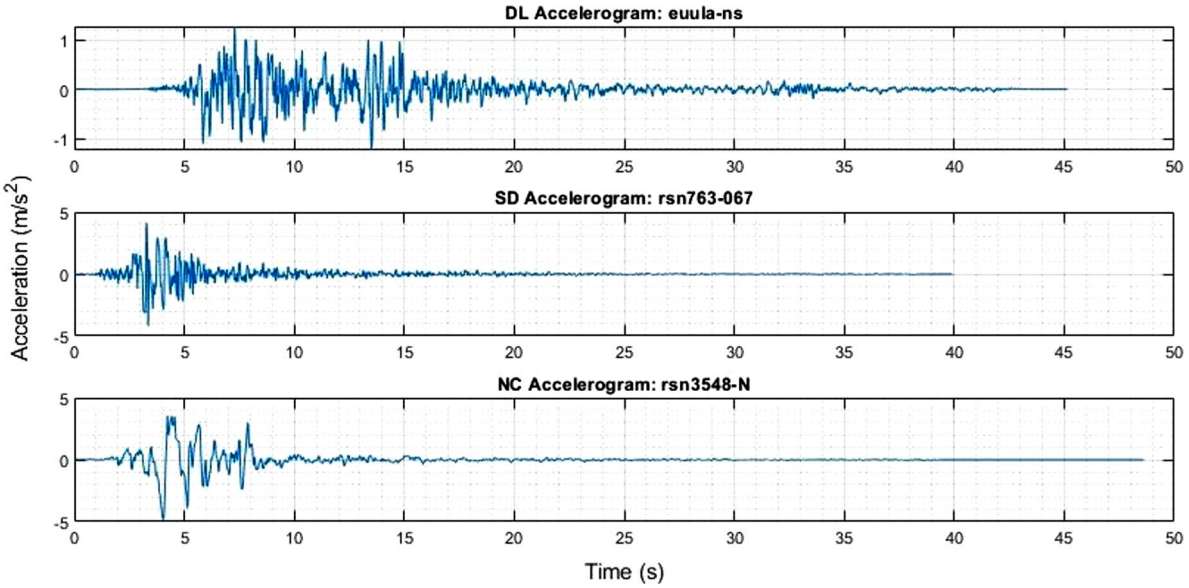


FIGURE 11 Seismic records adopted for HSs at DL, SD and NC limit states, respectively

phase and amplitude differences, whilst NENERR only to amplitude. Hence, the following errors were considered for the selection of the best candidate record for each limit state:

- Percentage error of the total hysteretic energy dissipated by the structure;
- NRMSE and NENERR of the base shear history;
- NRMSE and NENERR of the bending moment history on the joints at the first floor;
- NRMSE and NENERR of the horizontal displacement history at the first floor.

As a result, Table 9 reports the numerical values of the parameters related to the three different limit states in terms of errors between the responses of the monolithic and the sub-structured frame. For the DL limit state, the error is in the order of 20% considering all the parameters, whereas for the SD and the NC, the average error between all parameters is less than 10%; overall errors are acceptable. The selected records to be used in HS for DL, SD and NC limit states can be appreciated in Figure 11.

6.2 | HS programme

To investigate the seismic response of the full-scale frame equipped with DRBeS devices, the following test programme was conceived and carried out.

10969845, 0, Downloaded from https://onlinelibrary.wiley.com/doi/10.1002/eqe.3744 by CochraneItalia, Wiley Online Library on [03/11/2022]. See the Terms and Conditions (https://onlinelibrary.wiley.com/terms-and-conditions) on Wiley Online Library for rules of use; OA articles are governed by the applicable Creative Commons License

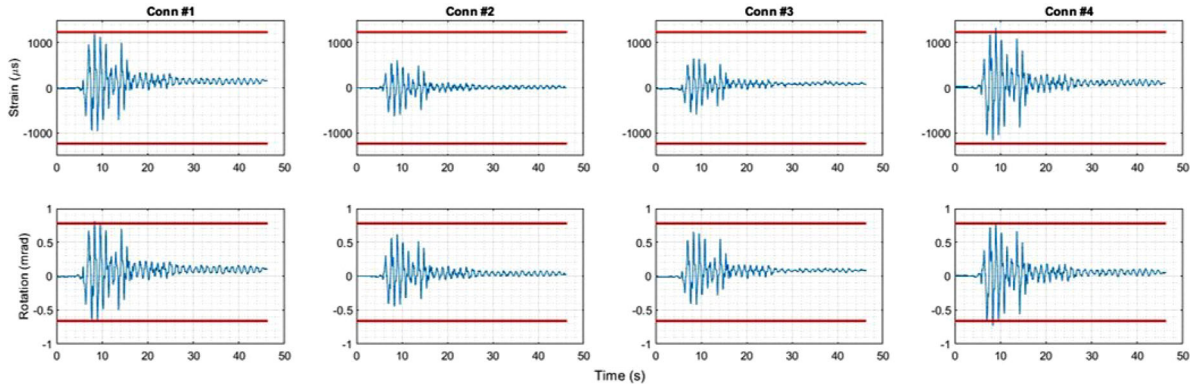


FIGURE 12 Flange plate strains and rotations of physical DRBeS connections at the DL state

1. HS at the **DL** limit state. After the test, the elastic behaviour of all dissipative devices and of the structural members was checked. Based on the results at the DL limit state, the numerical model was updated by varying the stiffness parameters of devices.
2. Test at the **SD** limit state. After the test, the elastic and the inelastic behaviour of the dissipative components and of the structural members was checked. Based on the outcomes, the possibility to update the numerical strength/damage parameters of the devices was also checked.
3. The damaged DRBeS plates were then replaced with new ones. The self-centering capability of the prototype building was verified and the residual inter-storey drift was measured.
4. Test at the **NC** limit state.

7 | RESULTS OF HYBRID SIMULATIONS

For each limit state, main results and comments of the PS are reported herein.

7.1 | Main results at the DL limit state

At the DL limit state, both the primary structural elements and the DRBeS of the PS remained in the elastic range. This trend can be inferred from the measurements of relative displacements; in fact both strains of the four flange plates composing each dissipative device and rotations of the four dissipative connections depicted in Figure 12, show that the yield limits, that is, red lines, were almost approached but not exceeded.

Here, the yield strain was estimated to be 1234.3 μs, whilst the connection yield rotations were estimated to be 0.78 and 0.66 mrad for sagging and hogging rotations, respectively. They were computed according to the provisions of the INNOSEIS project,[21] without considering slip due to bolt clearance, since tightened friction bolts were employed.

Consistently with no damage in the fuses of DRBeS, no damage was also observed in the irreplaceable parts of the frame, that is, reinforcement bars and column bases. In this respect, Figure 13 shows that the yield strain value of 2100 μs of the reinforcement bars and the elastic bending moment at the column bases were far from being exceeded. In fact, the elastic bending moment of the column member approached 436.2 kNm. Along this line, Figure 14 depicts the moment–rotation behaviour of all four connections Conn #1–Conn #4: this confirms with good approximation their linear behaviour at the DL limit state.

7.2 | Main results at the SD limit state

The HS at the SD limit state entailed, as expected, plastic deformations on the dissipative components that were detected from the sensors that measure relative displacements. In particular, Figure 15 shows that the yield limits were exceeded both for the strains in the flange plates of the devices and the rotations of the connections. Nonetheless, as expected, the

10969845, 0, Downloaded from https://onlinelibrary.wiley.com/doi/10.1002/eqe.3744 by CochraneItalia, Wiley Online Library on [03/11/2022]. See the Terms and Conditions (https://onlinelibrary.wiley.com/terms-and-conditions) on Wiley Online Library for rules of use; OA articles are governed by the applicable Creative Commons License

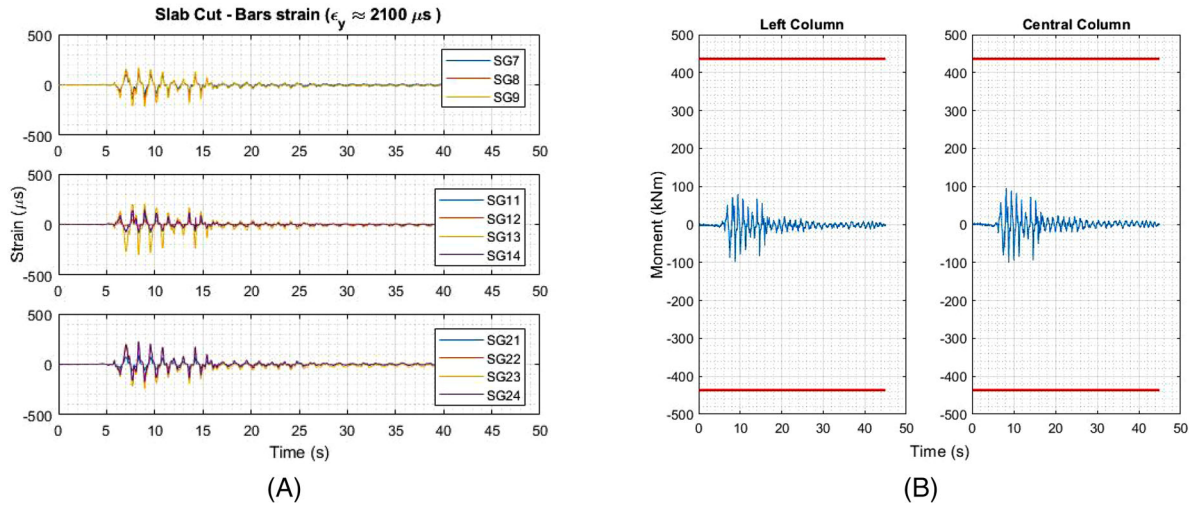


FIGURE 13 Irreplaceable components: (A) reinforcement bars strain and (B) bending moment at the base of the columns at the DL state

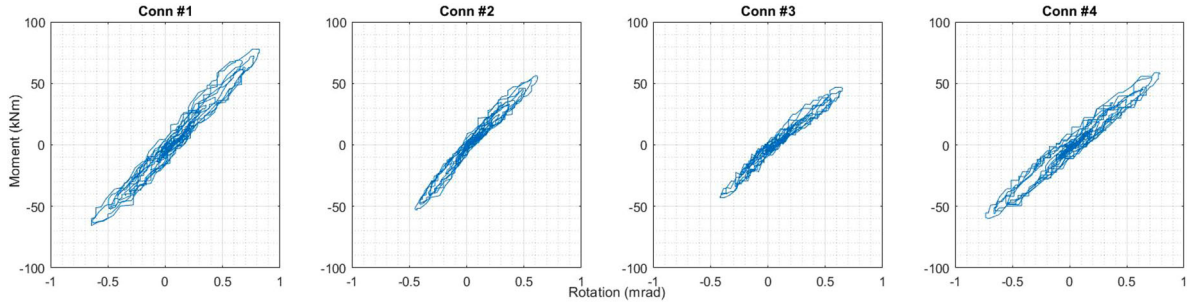


FIGURE 14 Experimental moment–rotation relationships at the DL limit state

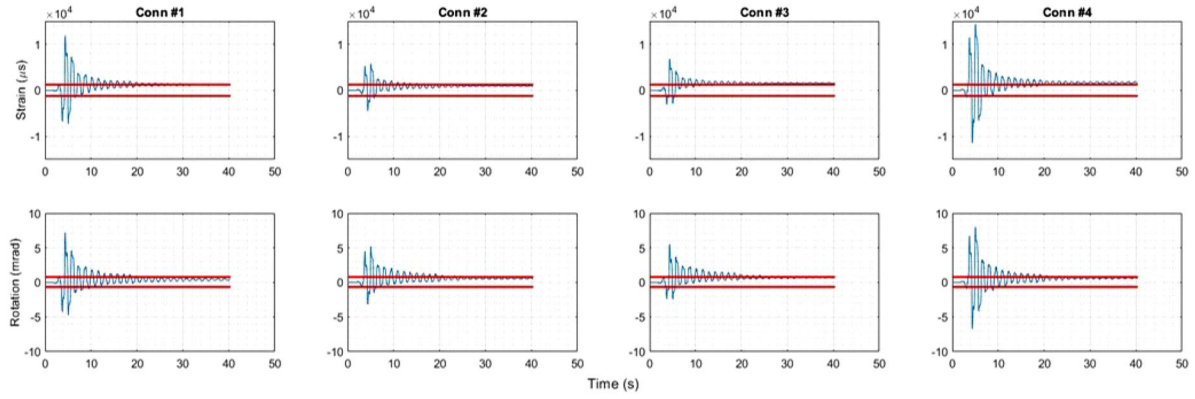


FIGURE 15 Flange plate strains and rotation of physical DRBeS connections at the SD limit state

non-dissipative irreplaceable parts of the frame remained undamaged after each HS and this is in line with the primary objective of the test campaign. This trend, indeed, can be observed from the measurements of the reinforcement bar strains and the estimated base column bending moments, all depicted in Figure 16. A careful reader can observe that the examined values remained below the yield strain threshold and the elastic bending moment threshold, respectively. The moment–rotation diagrams of Conn #1 and Conn #4 are depicted in Figure 17; they exhibit inelastic deformations with favourable hysteretic behaviour without significant loss of stiffness and strength.

Furthermore, photos of parts of the PS during the peak response of the PS are reported in Figure 18. All connections and joints appear to be intact; only a closer look indeed to the flange plate of Conn #4 reveals a slight damage of the

10969845, 0, Downloaded from https://onlinelibrary.wiley.com/doi/10.1002/eqe.3744 by CochraneItalia, Wiley Online Library on [03/11/2022]. See the Terms and Conditions (https://onlinelibrary.wiley.com/terms-and-conditions) on Wiley Online Library for rules of use; OA articles are governed by the applicable Creative Commons License

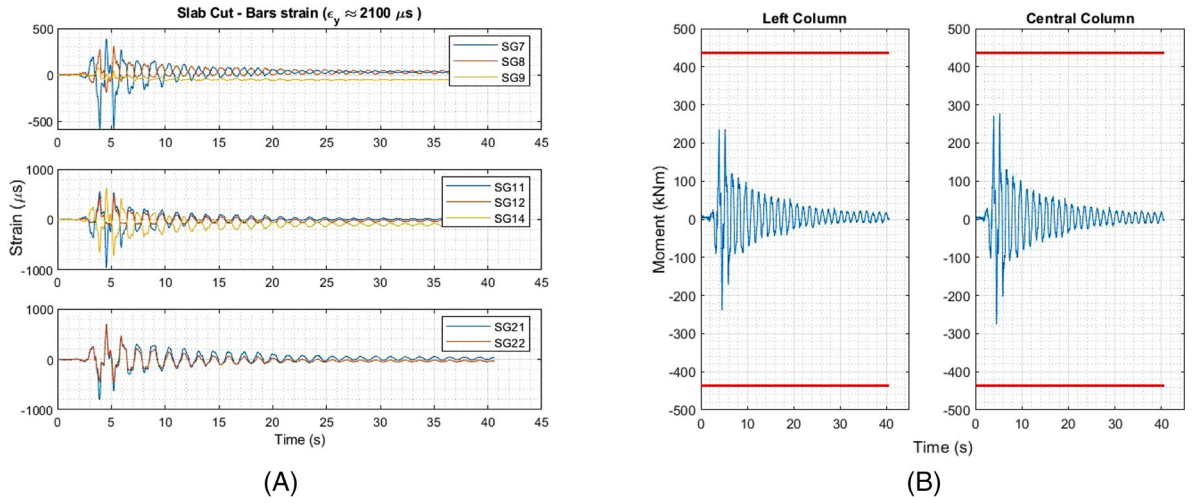
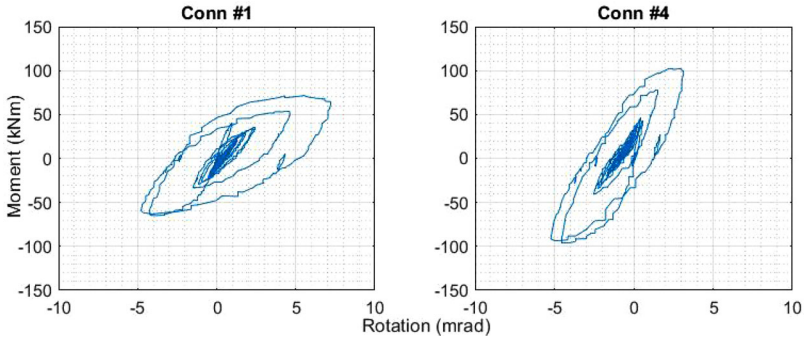


FIGURE 16 Irreplaceable components: (A) reinforcement bars strain histories (B) bending moment values at the base of the columns at the SD limit state

FIGURE 17 Experimental moment–rotation values of Conn #1 and Conn #4 at the SD limit state



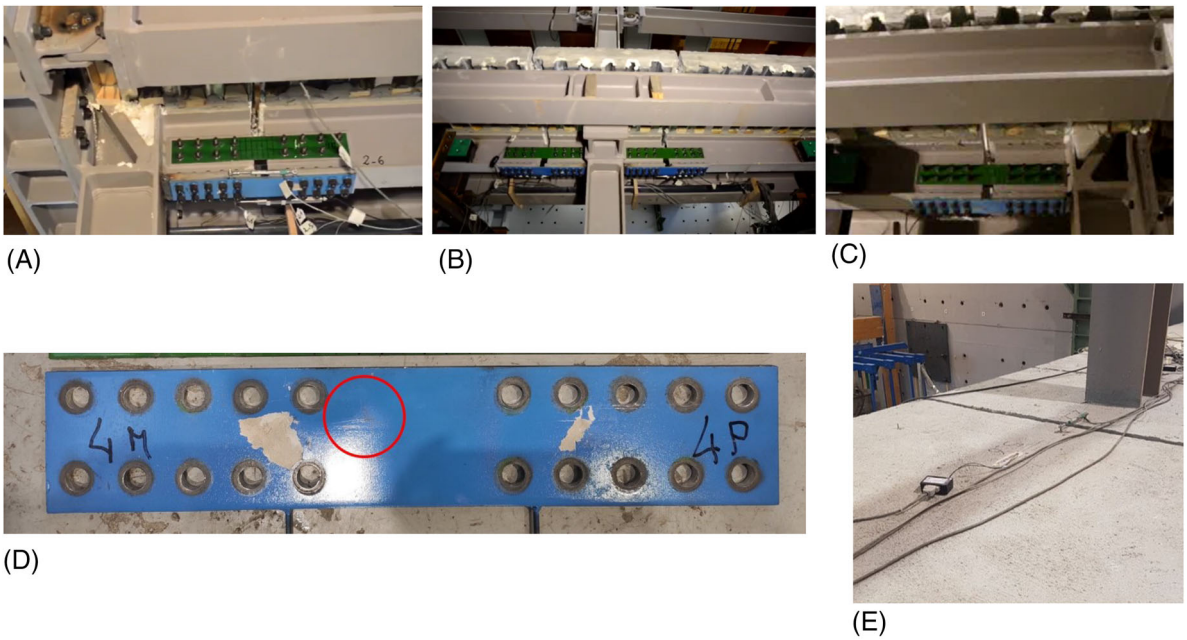


FIGURE 18 Conn #4 (A), Conns #3 and #2 (B) and Conn #1 (C) during the SD peak response; flange beam splice for Conn #4 after the SD limit state test (D); slab above Conn #3 (E) after the SD limit state test

10969845, 0, Downloaded from https://onlinelibrary.wiley.com/doi/10.1002/eqe.3744 by CochraneItalia, Wiley Online Library on [03/11/2022]. See the Terms and Conditions (https://onlinelibrary.wiley.com/terms-and-conditions) on Wiley Online Library for rules of use; OA articles are governed by the applicable Creative Commons License

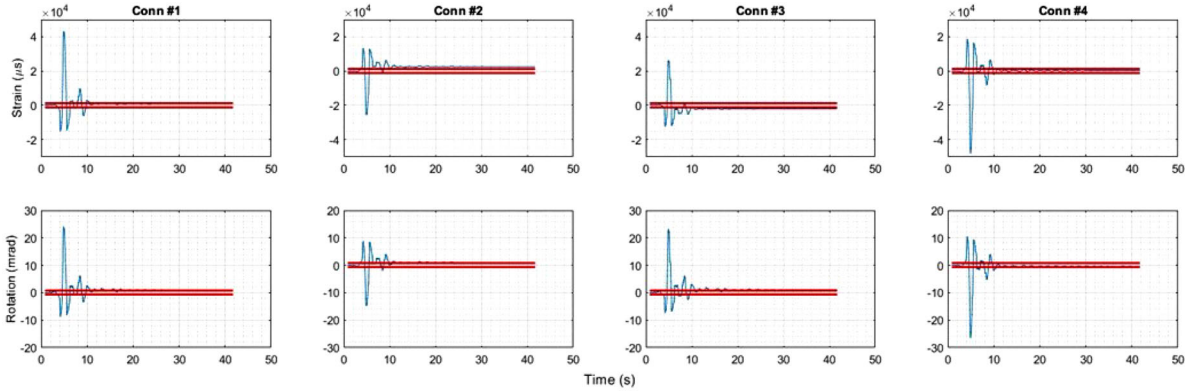


FIGURE 19 Flange plate strain and rotation histories of physical DRBeS connections at the NC limit state

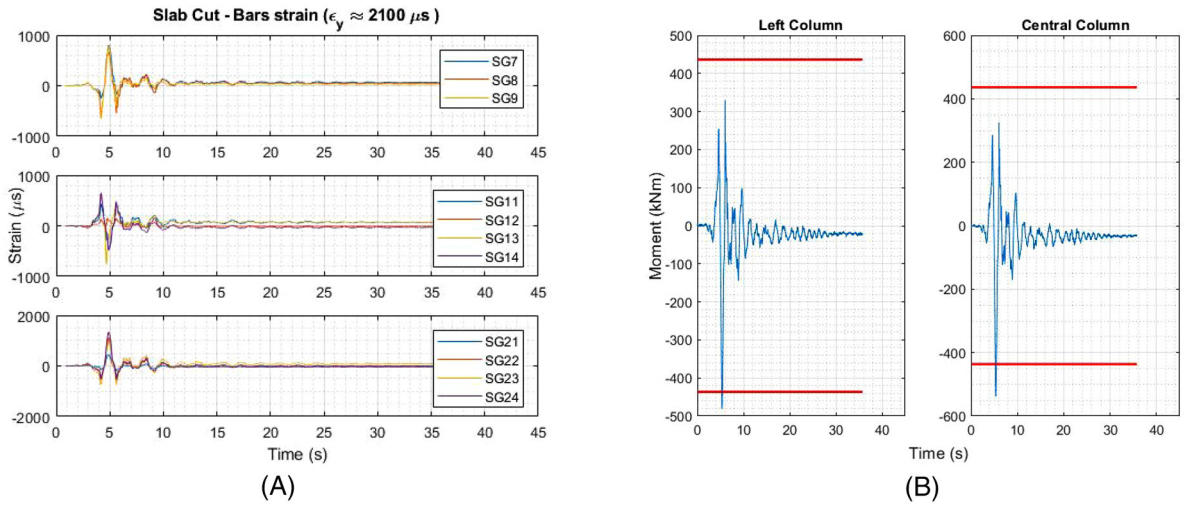


FIGURE 20 Irreplaceable components: (A) reinforcement bars strain histories; (B) bending moment values at the base of columns at the NC limit state

painting. As expected, the plates of the DRBeS devices could be easily dismounted and new plates could be installed for the subsequent test at the NC limit state.

7.3 | Main results at the NC limit state

Since the building was designed at the SD limit state, see Section 3 in this respect, at the NC limit state, the frame response including the PS was characterized by large hysteretic behaviour of partial-strength joints and yielding of some members. In fact, the connection rotations and the flange plate strains depicted in Figure 19 highlight that the fuses of DRBeS devices underwent large inelastic deformations. In particular, one can note that the compression strains of the flange plate entailed plate buckling under hogging rotations. Connecs #1, #2 and #4 were capable of protecting the irreplaceable parts, for example, the slab. Conversely, as depicted in Figure 22, the slab portion at the beam-to-column joint above Conn #3 was damaged and cracks appeared during the peak response. Nonetheless, the strain of the reinforcement bars remained below the yield value, as indicated in Figure 20.

Figure 20 depicts the bending moment at the column bases, which, for the central column, exceeded the elastic resisting moment of 23%. Again, Figure 21 shows the estimated moment–rotation diagrams of two connections, that is, Conn #1 and Conn #4 which highlight wide and stable hysteretic behaviours under seismic loads. Consistently with the ground motion record, the peak response was reached for sagging bending moment in Conn #1 and for hogging bending moment in Conn #4. As shown, the hogging behaviour of Conn #4 exhibited typical softening owing to plate buckling, which was

10969845, 0, Downloaded from https://onlinelibrary.wiley.com/doi/10.1002/eqe.3744 by CochraneItalia, Wiley Online Library on [03/11/2022]. See the Terms and Conditions (https://onlinelibrary.wiley.com/terms-and-conditions) on Wiley Online Library for rules of use; OA articles are governed by the applicable Creative Commons License

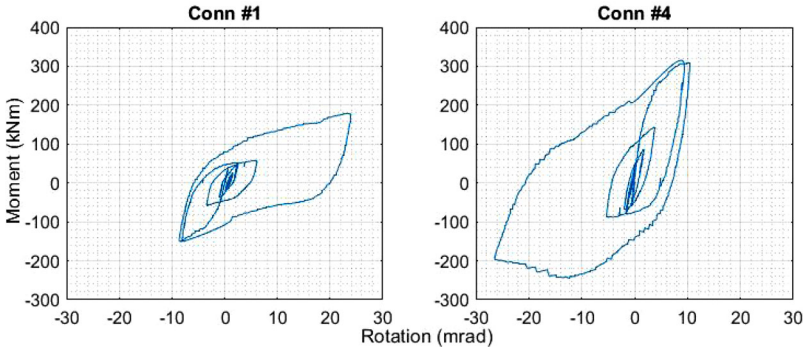


FIGURE 21 Experimental moment–rotation values of Conn #1 and Conn #4 at the NC limit state

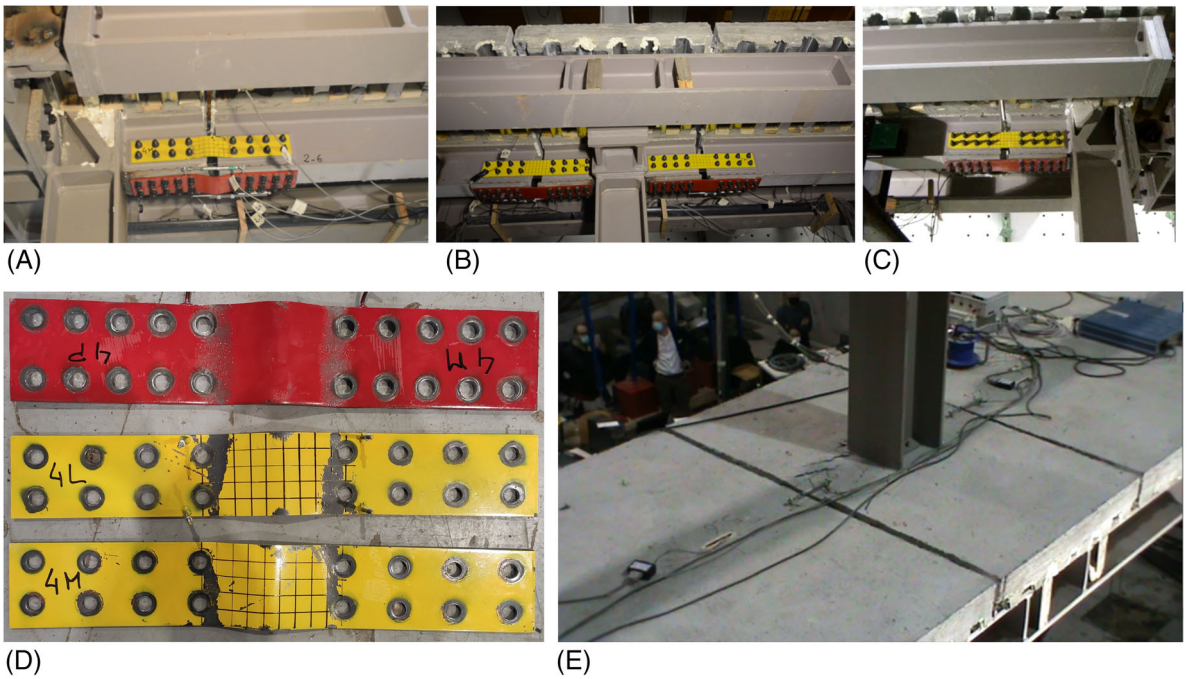


FIGURE 22 Conn #4 (A), Conns #3 and #2 (B) and Conn #1 (C) during the NC peak response; web and flange beam splices for Conn #4 after the NC limit state test (D); slab above Conn #3 (E) after the NC limit state test

TABLE 10 Residual actuator displacements and inter-storey drifts after the DL, SD and NC hybrid simulation

Actuator	DL	SD	NC
MOOG #1	0.0 mm (0.0‰)	0.3 mm (0.1‰)	2.4 mm (0.7‰)
MOOG #3	0.0 mm (0.0‰)	0.1 mm (0.0‰)	3.9 mm (4.3‰)

already highlighted by Calado[31] and Castiglioni.[32] The two external connections, namely Conn #1 and #4, were able to reach ultimate rotations of 23.9 and 26.5 mrad, respectively, without approaching collapse. Such rotations were achieved without ovalization of the bolt holes even for NC limit state test, as shown in Figure 22; this aspect is another positive experimental outcome in terms of replaceability.

To compare the frame response in terms of base shear versus top floor displacement history, Figure 23 superimposes, for each DL, SD and NC limit state, the aforementioned curves to the pushover response provided by the OpenSees reference model. One can observe that experimental data are in good agreement with the reference model prediction. Finally, the residual drifts and the inter-storey drift ratios are collected in Table 10. A reader can observe that for the DL limit state, no residual drift was measured, thus entailing an elastic behaviour. Conversely, both for the SD and NC limit states, some limited residual deformations of the frame were detected, thus highlighting a good re-centering capability of the steel–concrete composite system.

10969845, 0, Downloaded from https://onlinelibrary.wiley.com/doi/10.1002/eqe.3744 by CochraneItalia, Wiley Online Library on [03/11/2022]. See the Terms and Conditions (https://onlinelibrary.wiley.com/terms-and-conditions) on Wiley Online Library for rules of use; OA articles are governed by the applicable Creative Commons License

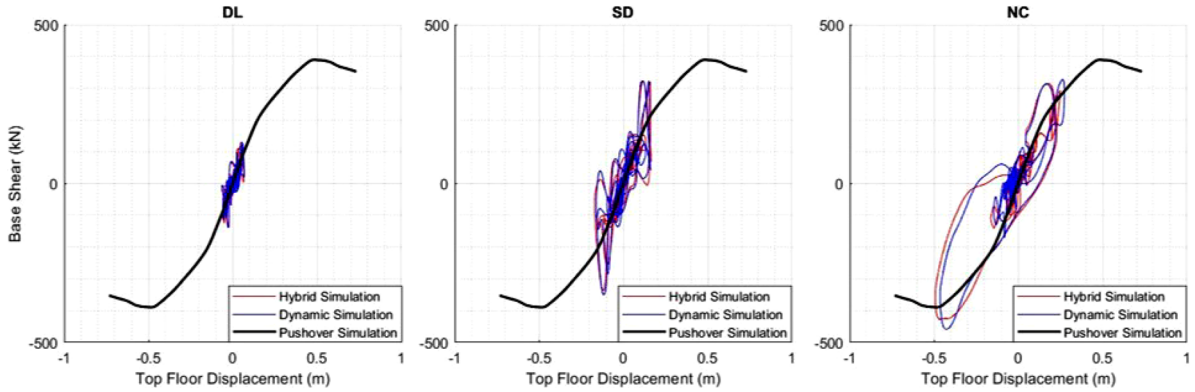


FIGURE 23 Base shear versus the top (6)th floor displacement relevant to the DL (A), SD (B) and NC (C) limit state HS. Comparison between HS and OpenSees pushover predictions

8 | CONCLUSIONS

The paper comprehensively described the results of extensive HS on full-scale partial-strength steel–concrete composite moment-resisting frames (MRFs) equipped with DRBeS. Within the PBEE approach, three limit states relevant to specific seismic inputs have been considered: namely DL, SD and NC. More specifically and anew within the PBEE approach, ease of replacement of the components after the SD limit state was assessed. The main outcomes of the research are summarized herein.

- At the DL limit state, the whole MRF behaved elastically without any damage suffered by the dissipative components, and the residual drift was practically zero.
- At the SD limit state, energy dissipation in the beam splices composing the DRBeS was detected with no damage in the non-replaceable parts of the frame. The DRBeS exhibited favourable inelastic behaviour without appreciable loss of stiffness and strength. Plate buckling was not visible and only slight damage was observed. Dismounting of the damaged plates and replacement with the new ones were easily achieved.
- At the NC limit state, the DRBeS were highly damaged with evident plate buckling due to hogging bending moments. The hysteretic behaviour of the components was characterized by large cycles with a softening branch at large rotations. Since the structure was designed to cope with the SD limit state, some damage in the non-dissipative parts was observed: more precisely, cracking in the concrete slab and some yielding in the column bases. However, the overall behaviour was satisfactory with small residual inter-storey drifts and a favourable re-centering capability.
- The HS was successfully implemented by means of a G-α algorithm and the Craig–Bampton component mode synthesis. Indeed, the HSs were capable of well reproducing the whole seismic response of the six-story MRF frame. Moreover, the pushover curves obtained from the reference model agreed well with the global quantities of force feedback and actuator displacements. In addition, also the local quantities in terms of moments and rotations were in agreement with the predictions of the numerical models, though the prediction of component behaviours from global full-scale tests remains a not trivial issue.

Overall, it was shown that the favourable properties of partial-strength steel–concrete composite MRFs equipped dowed with DRBeS. Though slab reinforcements and the relevant composite slab were damaged beyond the SD limit state, the detailing of the proposed partial-strength beam-to-column joints deserves further studies. And what's more, fire behaviour of multi-storey buildings typically assumes good compartmentalization between floors; this also applies to steel frames designed in highly seismic regions.[46] To minimise the potential spread of fire among the floors which may cause severe damage and be critical to structural stability, at the very least, the fire compartmentalization of a building equipped with DRBeS should be carefully analysed because of the cut through the slab.

ACKNOWLEDGEMENTS

This work was carried out with a financial grant from the Research Fund for Coal and Steel of the European Union, within the DISSIPABLE project: 'Fully dissipative and easily repairable devices for resilient buildings with composite

10969845, 0, Downloaded from https://onlinelibrary.wiley.com/doi/10.1002/eqe.3744 by CochraneItalia, Wiley Online Library on [03/11/2022]. See the Terms and Conditions (https://onlinelibrary.wiley.com/terms-and-conditions) on Wiley Online Library for rules of use; OA articles are governed by the applicable Creative Commons License

steel–concrete structures', Grant No. 800699-RFCS-2017; and from the Italian Ministry of Education, University and Research (MIUR) in the frame of the Departments of Excellence (Grant L232/2016).

DATA AVAILABILITY STATEMENT

The data that support the findings of this study are available from the corresponding author upon reasonable request.

ORCID

Roberto Andreotti https://orcid.org/0000-0001-6895-9152
Giulia Giuliani https://orcid.org/0000-0002-7085-6408
Nicola Tondini https://orcid.org/0000-0003-2602-6121
Oreste S. Bursi https://orcid.org/0000-0003-3072-7414

REFERENCES

1. Li W, Li Q, Jiang W, Jiang L. Seismic performance of composite reinforced concrete and steel moment frame structures – state-of-the-art. *Compos Part B: Eng*. 2011;42:190-206.
2. Elnashai A, Di Sarno L. *Fundamentals of Earthquake Engineering*. John Wiley & Sons, Ltd; 2008.
3. Macedo L, Castro J. Earthquake loss assessment of steel moment-resisting frames designed according to Eurocode 8. *Soil Dyn Earthq Eng*. 2019;124:58-71.
4. Ministry of Infrastructures and Transportations. *Norme Tecniche per le costruzioni, DM 18 Gennaio 2018*. Ministry of Infrastructures and Transportations; 2018.
5. CEN. *EN 1998-1 – Eurocode 8: Design of Structures for Earthquake Resistance – Part 1: General Rules, Seismic Actions and Rules for Buildings*. CEN – European Committee of Standardization; 2004.
6. CEN. *EN 1998-1 – Eurocode 8 – Design of Structures for Earthquake Resistance – Part 1: General Rules, Seismic Actions and Rules for Buildings. Working Draft*. CEN – European Committee of Standardization; 2018.
7. CEN. *EN 1993-1-8 – Eurocode 3 – Design of Steel Structures – Part 1-8: Design of Joints. 2nd Draft*. CEN – European Committee of Standardization; 2017.
8. ANSI/AISC. *ANIS/AISC 341-16 – Seismic Provisions for Structural Steel Buildings*. American Institute Of Steel Construction; 2016.
9. JSCE. *JSCE – Standard Specifications for Steel and Composite Structures*. Japan Society of Civil Engineers; 2007.
10. Cornell C, Krawinkler H. Progress and challenges in seismic performance assessment. *PEER Center News*. 2000, 3.
11. Pucinotti R, Tondini N, Zanon G, Bursi O. Tests and model calibration of high-strength steel tubular beam-to-column and column-base composite joints for moment-resisting structures. *Earthq Eng Struct Dyn*. 2015;44:1471-1493.
12. Tondini N, Zanon G, Pucinotti R, Di Filippo R, Bursi O. Seismic performance and fragility functions of a 3D steel-concrete composite structure made of high-strength steel. *Eng Struct*. 2018;174:373-383.
13. Montuori R, Nastri E, Piluso V, Troisi M. Influence of connection typology on seismic response of MR-Frames with and without "set-backs". *Earthq Eng Struct Dyn*. 2017;46:5-25.
14. Soong T. *Active Structural Control: The Theory and Practice*. Longman Scientific and Technical; 1991.
15. Di Benedetto S, Francavilla A, Latour M, Piluso V, Rizzano G. Experimental response of a large-scale two-storey steel building equipped with low-yielding friction joints. *Soil Dyn Earthq Eng*. 2021;152. https://doi.org/10.1016/j.soildyn.2021.107022
16. Piluso V, Montuori R, Nastri E, Paciello A. Seismic response of MRF-CBF dual systems equipped with low damage friction connections. *J Constr Steel Res*. 2019;135:123-136.
17. Freddi F, Dimopoulos C, Karavasilis T. Experimental evaluation of a rocking damage-free steel column base with friction devices. *J Struct Eng*. 2020;146. https://doi.org/10.1061/(ASCE)ST.1943-541X.0002779
18. Chan RWK, Albermani F. Experimental study of steel slit damper for passive energy dissipation. *Eng Struct*. 2007;30:1058-1066.
19. Oh SH, Kim YJ, Ryu HS. Seismic performance of steel structures with slit dampers. *Eng Struct*. 2009;31:1997-2008.
20. Koetaka Y, Chusilp P, Zhang Z, et al. Mechanical property of beam-to-column moment connection with hysteretic dampers for column weak axis. *Eng Struct*. 2005;27:109-117.
21. Vayas I. *Innovative Anti-seismic Devices and Systems*. ECCS – European Convention for Constructional Steelwork; 2017.
22. Plumier A, Doneux C, Castiglioni C, et al. *Two Innovations for Earthquake-resistant Design: The INERD Project – Final Report*. Technical Report. Université de Liège – Institut de Mécanique et Génie Civil, Politecnico di Milano – Dipartimento di Ingegneria Strutturale, Instituto Superior Técnico Lisboa – Department of Civil Engineering and Architecture, University of Trento – Dipartimento di Ingegneria Mecc. e Strutturale, NTUA – National Technical University of Athens – Department of Civil Engineering, ProfilArbed Recherches; 2004.
23. Vayas I, Karydakis P, Dimakogianni D, et al. *Dissipative Devices for Seismic Resistant Steel Frames (Fuseis) – Final Report*. Technical Report. National Technical University of Athens, Politecnico di Milano, Instituto Superior Técnico Lisboa, RWTH Aachen University, SIDENOR SA; 2011.
24. Mahmoud H, Elnashai A, Spencer B, Kwon O, Bennier DJ. Hybrid simulation for earthquake response of semirigid partial-strength steel frames. *J Struct Eng*. 2013;139(7):1134-1148.
25. Xu G, Wang Z, Wu B, et al. Pseudodynamic tests with substructuring of a full-scale precast box-modularized structure made of reinforced concrete shear walls. *Struct Des Tall Special Build*. 2017;26:e1354.

10969845, 0, Downloaded from https://onlinelibrary.wiley.com/doi/10.1002/eqe.3744 by CochraneItalia, Wiley Online Library on [03/11/2022]. See the Terms and Conditions (https://onlinelibrary.wiley.com/terms-and-conditions) on Wiley Online Library for rules of use; OA articles are governed by the applicable Creative Commons License

26. Del Carpio M, Mosqueda G, Lignos D. Experimental investigation of steel building gravity framing systems under strong earthquake shaking. *Soil Dyn Earthq Eng*. 2019;116:230-241.
27. Abbiati G, Bursi OS, Caperan P, et al. Hybrid simulation of multi-span RC viaduct with plain bars and sliding bearings. *Earthq Eng Struct Dyn*. 2015;44:2221-2240.
28. Bursi OS, Abbiati G, Cazzador E, et al. Nonlinear heterogeneous dynamic substructuring and partitioned FETI time integration for the development of low-discrepancy simulation models. *Int J Numer Methods Eng*. 2017;112:1253-1291.
29. Kanyilmaz A, Castiglioni CA. *Dissipable Proposal*. Technical Report. Politecnico di Milano, Instituto Superior Técnico Lisboa, University of Trento, RWTH Aachen University, National Technical University of Athens NTUA, RINA Consulting – Centro Sviluppo Materiali SpA, University of Pisa, SOFMAN; 2017.
30. Calado L, Proenca JM, Espinha M, Castiglioni CA. Hysteretic behaviour of dissipative welded fuses for earthquake resistant steel frames. *Steel Compos Struct*. 2013;14(6):547-569.
31. Calado L, Proenca JM, Espinha M, Castiglioni CA. Hysteretic behaviour of dissipative bolted fuses for earthquake resistant steel frames. *J Constr Steel Res*. 2013;85:151-162.
32. Castiglioni CA, Kanyilmaz A, Calado L. Experimental analysis of seismic resistant composite steel frames with dissipative devices. *J Constr Steel Res*. 2012;76:1-12.
33. Kanyilmaz A, Castiglioni CA, Drei A, Vayas I, Calado L, Rauert T. Nonlinear dynamic response of dissipative devices for seismic resistant steel frames: experimental behavior and numerical simulation. In: Proceedings of the COMPDYN 2011, Corfu, Greece. 2011.
34. Kanyilmaz A, Castiglioni C. Performance of multi-storey composite steel-concrete frames with dissipative fuse devices. In: Proceedings of the COMPDYN 2015, Crete Island, Greece; 2015.
35. Valente M, Castiglioni CA, Kanyilmaz A. Dissipative devices for earthquake resistant composite steel structures: bolted versus welded solution. *Bull Earthq Eng*. 2016;14:3613-3639.
36. CEN. *EN 1993-1-1 – Eurocode 3: Design of Steel Structures – Part 1–1: General Rules and Rules for Buildings*. CEN – European Committee of Standardization; 2005.
37. CEN. *EN 1993-1-8 – Eurocode 3: Design of steel structures – Part 1-8: Design of Joints*. CEN – European Committee of Standardization; 2005.
38. CEN. *EN 1994-1 - Eurocode 4: Design of Composite Steel and Concrete Structures – Part 1.1: General Rules, and Rules for Buildings*. CEN – European Committee of Standardization; 2004.
39. McKenna F, Fenves GL, Scott M. *OpenSees: Open System for Earthquake Engineering Simulation*. University of California Berkeley; 2006. http://opensees.berkeley.edu
40. Andreotti R, Giuliani G, Tondini N, Bursi OS. Dynamic substructuring tests of steel frames equipped with easily repairable dissipative seismic devices. In: Proceedings of the 17th World Conference on Earthquake Engineering, Sendai, Japan; 2020.
41. Lowes LN, Mitra N, Altoontash A. *A Beam-Column Joint Model for Simulating the Earthquake Response of Reinforced Concrete Frames*. Technical Report. University of Washington, Stanford University; 2004.
42. Chisari C, Francavilla A, Latour M, Piluso V, Rizzano G, Amadio C. Critical issues in parameter calibration of cyclic models for steel members. *Eng Struct*. 2017;132:123-138.
43. Abbiati G, Lanese I, Cazzador E, Bursi OS, Pavese A. A computational framework for fast-time hybrid simulation based on partitioned time integration and state-space modeling. *Struct Control Health Monit*. 2019;26:e2419.
44. Craig RR, Kurdila A. *Fundamentals of Structural Dynamics*. John Wiley & Sons, Inc; 2006.
45. Abbiati G, Covi P, Tondini N, Bursi O, Stojadinovic B. A real-time hybrid fire simulation method based on dynamic relaxation and partitioned time integration. *J Eng Mech*. 2020;146(9). https://doi.org/10.1061/(ASCE)EM.1943-7889.0001826
46. Possidente L, Weiss A, Silva dD, Pustorino S, Nigro E, Tondini N. Fire safety engineering principles applied to a multi-storey steel building. *Proc Inst Civ Eng-Struct Build*. 2021;174(9):752-738.

How to cite this article: Andreotti R, Giuliani G, Tondini N, Bursi OS. Hybrid simulation of a partial-strength steel–concrete composite moment-resisting frame endowed with hysteretic replaceable beam splices. *Earthquake Engng Struct Dyn*. 2022;1-20. https://doi.org/10.1002/eqe.3744

10969845, 0, Downloaded from https://onlinelibrary.wiley.com/doi/10.1002/eqe.3744 by CochraneItalia, Wiley Online Library on [03/11/2022]. See the Terms and Conditions (https://onlinelibrary.wiley.com/terms-and-conditions) on Wiley Online Library for rules of use; OA articles are governed by the applicable Creative Commons License